Available online at www.sciencedirect.com

ScienceDirect

Scripta Materialia 75 (2014) 102–105

Scripta MATERIALIA

www.elsevier.com/locate/scriptamat

Evolution of plasticity, strain-rate sensitivity and the underlying deformation mechanism in Zn–22% Al during high-pressure torsion

In-Chul Choi,[a] Yong-Jae Kim,[a] Byungmin Ahn,[b] Megumi Kawasaki,[a,*] Terence G. Langdon[c,d] and Jae-il Jang[a,*]

[a]*Division of Materials Science and Engineering, Hanyang University, Seoul 133-791, South Korea*

[b]*Department of Energy Systems Research, Ajou University, Suwon, 443-749, South Korea*

[c]*Departments of Aerospace & Mechanical Engineering and Materials Science, University of Southern California, Los Angeles, CA 90089-1453, USA*

[d]*Materials Research Group, Faculty of Engineering and the Environment, University of Southampton, Southampton SO17 1BJ, UK*

Received 11 October 2013; revised 29 November 2013; accepted 2 December 2013
Available online 7 December 2013

This study explores the evolution of plasticity, strain-rate sensitivity and the underlying deformation mechanism of a Zn–22% Al eutectoid alloy during high-pressure torsion processing. The experiments reveal an optimal torsional straining condition for achieving the largest plasticity; beyond this condition the strain-rate sensitivity decreases and activation volume increases. The results are discussed in terms of changes in the microstructure and the underlying deformation mechanism.

Keywords: Zn–Al alloy; High-pressure torsion; Strain-rate sensitivity; Deformation mechanism; Nanoindentation

It is well known that the Zn–Al eutectoid alloy exhibits significant elongations at room temperature (RT) due to its low melting temperature T_m where RT corresponds to $\sim 0.44T_m$ [1]. Recently, it was also reported that the high-temperature superplasticity of this alloy can be significantly enhanced by reducing the grain size via severe plastic deformation processing [2,3], such as through equal-channel angular pressing (ECAP) [4] or high-pressure torsion (HPT) [5]. The processing of disks by HPT is especially attractive because it induces grain sizes that are smaller than those produced by ECAP [6]. During HPT, the equivalent strain ε_{eq} imposed on the disk is given by the relationship [7]:

$$\varepsilon_{eq} = \frac{2\pi N r}{h\sqrt{3}} \quad (1)$$

where r and h are the radius and thickness of the disk and N is the number of torsional revolutions. Thus, the strain varies locally across the disk; this contrasts with ECAP where the strain is reasonably constant.

Extensive research has been performed to elucidate the evolution of microstructure and hardness of Zn–Al alloys during HPT processing at RT [8,9]. Nevertheless, no attempt has been made to monitor the change in plastic deformation characteristics at RT during HPT processing. The strain-rate sensitivity, m, and activation volume, V^*, are useful quantitative indicators of the thermally activated plastic deformation including superplasticity and its predominant mechanism [10]. At decreasing length scale of materials, such as grain size or twin spacing, increasing m and lowering V^* are critical for delaying the development of stress concentrations [11].

The values of m and V^* can be estimated through nanoindentation testing which offers both a simple and easy testing procedure and the need for only a very small volume of material. In practice, the nanoindentation permits the collection of statistical data from a localized region for the hardness, H, and indentation strain rate, $\dot{\varepsilon}_i$, which may be used to estimate the flow stress, σ_f, and uniaxial strain rate, $\dot{\varepsilon}_{uni}$ [12–14], that are essential for determining m and V^*. Accordingly, the present study was initiated to explore the evolution of the m and V^* in a Zn–22% Al alloy during HPT processing through nanoindentation experiments.

The experiments were conducted with a commercial Zn–22 wt.% Al eutectoid alloy where the as-received alloy contained a binary microstructure with an Al-rich α phase and a Zn-rich β phase. Disk samples with

* Corresponding authors. Tel.: +82 222200402; fax: +82 222202294; e-mail addresses: megumi@hanyang.ac.kr; jijang@hanyang.ac.kr

1359-6462/$ - see front matter © 2013 Acta Materialia Inc. Published by Elsevier Ltd. All rights reserved.
http://dx.doi.org/10.1016/j.scriptamat.2013.12.003

thicknesses, t, of ~1.5–2.0 mm and diameters of 10 mm were annealed in air at 473 K for 1 h and then carefully polished on both sides to a final t of ~0.80 mm. The HPT processing was conducted at RT under quasiconstrained conditions [15] using a pressure of 6.0 GPa and a fixed speed of 1 rpm. The disks were processed for totals of 1, 2 or 4 turns. Then, to observe microstructure and grain size, all disks were prepared using an ion beam cross-section polisher (JEOL CP SM-09010), and examined by field-emission scanning electron microscopy (FE SEM; JEOL JSM-7001F). Detailed information on the microstructural analysis is provided elsewhere [8].

Nanoindentation experiments were performed at the edge of each disk at RT using a Nanoindenter-XP (formerly MTS; now Agilent, Oak Ridge, TN) with a three-sided pyramidal Berkovich indenter having a centerline-to-face angle of 65.3°. During the tests, the specimen was loaded to a fixed peak load $P_{max} = 20$ mN at different indentation rates $\dot{\varepsilon}_i = h^{-1}(dh/dt)$ of 0.0125, 0.025, 0.05 and 0.1 s^{-1}. Under each testing condition, more than 50 indentations were conducted to provide statistically validated hardness values. Thermal drift was maintained below 0.1 nm s^{-1} in all experiments and topological features of the indented surfaces were identified by FE SEM. Additionally, in situ indentation tests were conducted inside a Quanta 250 FEG SEM (FEI Inc., Hillsboro, OR) with a PI 85 Picoindenter (Hysitron Inc., Minneapolis, MN) under a fixed peak load of 10 mN at $dP/dt = 0.5$ mN s^{-1}.

Figure 1 shows SEM images of representative microstructures of (a) the as-annealed sample ($N = 0$) and near the edges of the disks after HPT for (b) 1, (c) 2 and (d) 4 turns. Inspection shows there are significant changes in the microstructural features with increasing N. The initial microstructure consists of homogeneously distributed α and β phases, which appear black and white, respectively, and there are areas both of equiaxed grains and of a lamellar structure. Thereafter, HPT processing removes the lamellar structure and induces a banded structure in which agglomerates of both Al-rich and Zn-rich equiaxed fine grains delineate the torsional flow pattern up to 2 turns as shown in Figure 1b and c. After 4 turns, as shown in Figure 1d, the distributions of Zn and Al grains are reasonably homogeneous and the banded structure has essentially disappeared. There were average grain sizes of ~1.4 μm in the annealed condition, ~400 nm after 1 turn, and ~350 nm after 2 and 4 turns at the edges of the HPT-processed disks. These grain sizes are consistent with previous TEM observations (~0.1–0.5 μm) [16].

Representative load–displacement (P–h) curves are given in Figure 2a where the main plot shows samples for $N = 0$ and 4 tested at four different $\dot{\varepsilon}_i$ and the inset shows all four samples tested at $\dot{\varepsilon}_i = 0.025$ s^{-1}. There are three important tendencies noticeable from these measurements. First, at any given indentation strain rate, the displacement at peak load increases with increasing N. Second, there is a significant rate dependency on the peak-load displacement. Third, remarkable indentation creep occurs during a very short holding sequence of only 1 s, thus suggesting excellent RT plasticity in this alloy.

From the P–h curves, the nanoindentation hardness, H, was estimated according to the Oliver–Pharr method [17]. In Figure 2b, variations in H with N are displayed for the alloy together with reported data of Vickers microhardness Hv on an identical HPT-processed alloy [8]. It should be noted that the values of Hv were recalculated as load divided by the projected area instead of surface area in order to provide a direct comparison with the values of H. Although the tendency of the change in H is almost the same for both sets of measurements, the H values in this work are slightly higher than the values calculated from Hv. This may be due to an indentation size effect which is manifested as an increase in H with decreasing indentation load P (and depth h) for sharp indentation; the $P_{max} = 20$ mN in this study is much lower than the value of ~980 mN in Ref. [8].

Two trends are apparent from Figure 2b. First, all HPT-processed disks show lower H values than the annealed condition and the H values continuously decrease with increasing N. This is due to the occurrence of HPT-induced weakening despite extensive grain refinement.

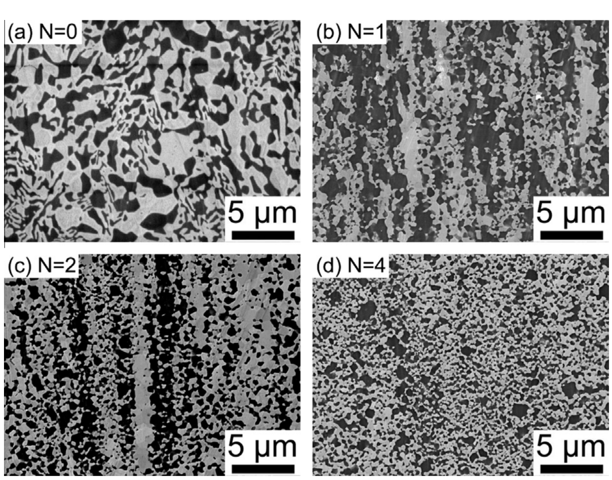

Fig. 1. Representative SEM images taken in the disk of (a) $N = 0$ and at the edge of the disks after HPT for (b) 1, (c) 2 and (d) 4 turns.

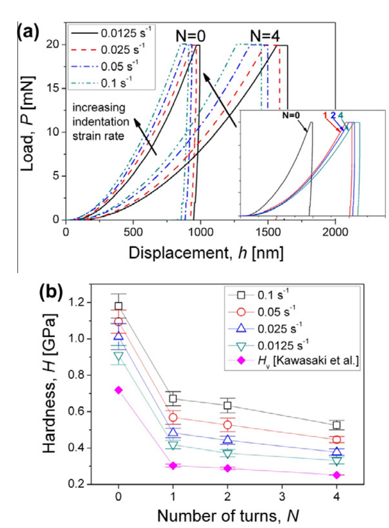

Fig. 2. (a) Typical P–h curves obtained at different indentation rates for the disks of $N = 0$ and 4 (an inset image shows the change in the curve with N at an indentation strain rate of 0.025 s^{-1}) and (b) hardness variation with increasing N (literature data from Ref. [8] are included for comparison purposes).

The phenomenon is readily explained by earlier TEM observations [16] in which HPT processing gave a significant reduction in the rod-shaped Zn precipitates which are visible within the Al-rich grains in the annealed condition. Thus, there is a significant loss in hardness of the Zn–Al alloy after processing and this hardness model, together with other models, was discussed recently for several metals and alloys [18].

Second, the measured hardness is rate sensitive as also shown in Figure 2a and dramatically increases with increasing $\dot{\varepsilon}_i$. The value of m is an important material property for understanding thermally activated deformation mechanisms and is often determined at a given strain, ε, and absolute temperature, T, by the expression [19]:

$$m = \left(\frac{\partial \ln \sigma_f}{\partial \ln \dot{\varepsilon}}\right)_{\varepsilon,T} = \left(\frac{\partial \ln(H/C)}{\partial \ln \dot{\varepsilon}}\right)_{\varepsilon,T} \quad (2)$$

where σ_f is the flow stress estimated by Tabor's empirical relation of $\sigma_f \approx H/C$, where C is a constraint factor of $\sim$3 for fully plastic deformation [12]. Applying the empirical relation for a strain rate of $\dot{\varepsilon} \approx 0.01\dot{\varepsilon}_i$ [13,14], the value of m was calculated for each material as the slope of the line in a logarithmic plot of $H/3$ vs. $\dot{\varepsilon}_i$ as shown in the small inset in Figure 3a. The variation in m with increasing N is shown as the main plot in Figure 3a. The estimated $m \approx 0.124$ for $N = 0$ is within the range between $\sim$0.15 for pure Zn [20] and $\sim$0.02 for pure Al [21] and is in excellent agreement with reported values of $\sim$0.125–0.15 at the tensile strain rates of $\sim 10^{-4}$–10^{-3} s^{-1} at RT for the Zn–Al alloy without processing [22]. Moreover, the HPT-processed samples show $m \approx 0.226$–0.256, which is consistent with reported values of $\sim$0.2–0.3 at RT for the Zn–Al alloy processed by ECAP [22]. These agreements imply that the nanoindentation technique gives an accurate value of m.

The most important feature in Figure 3a is the variation of m with N. The estimated m is enhanced significantly from $N = 0$ to 1 by a factor of 2 and increases slightly through 2 turns. However, m decreases with increasing N from 2 to 4. Such a transition in the m–N variation implies a change in the nature of plasticity in the Zn–Al alloy such that there is an optimal HPT straining condition for achieving the largest plasticity and thus the highest value of m.

The plastic deformation mechanism may be estimated from the value of the activation volume V^* which is given by:

$$V^* = \sqrt{3}kT\left(\frac{\partial \ln \dot{\varepsilon}}{\partial \sigma_f}\right) = \sqrt{3}kT\left(\frac{\partial \ln \dot{\varepsilon}}{\partial (H/C)}\right) \quad (3)$$

where k is Boltzmann's constant. The value of V^* may vary by orders of magnitude for different rate-limiting processes with typical values of V^* in the range of $\sim 100\boldsymbol{b}^3$ to $\sim 1000\boldsymbol{b}^3$ for dislocation glide of face-centered cubic metals [23], $\sim 10\boldsymbol{b}^3$ for grain boundary sliding (GBS) [24] and $\sim \boldsymbol{b}^3$ for grain boundary (GB) or lattice diffusion [23,25], where $\boldsymbol{b}$ is the Burgers vector.

Using Eq. (3), the value of V^* was estimated from the slope of a linear fit of logarithmic strain rate vs. linear flow stress as shown in the inset of Figure 3b and the results are summarized in the main plot of Figure 3b. The calculated values of V^* are ~ 8.5–$11.4\boldsymbol{b}^3$, where $\boldsymbol{b} \approx 2.7 \times 10^{-10}$ m for the Zn–22 wt.% Al alloy [26], and thus they are close to $\sim 10\boldsymbol{b}^3$ for all samples in the present experiments. This suggests GBS as the predominant deformation mechanism for both the unprocessed and HPT-processed samples. Nevertheless, it is apparent that the disk for $N = 4$ exhibits higher V^* than the other samples with no dependence on N. In practice, higher stresses are required to operate plastic deformation mechanisms with higher V^* and therefore it is concluded that the sample with $N = 4$ exhibits some activity which increases the value of V^* so that GBS becomes less active.

To evaluate the less-pronounced GBS in the sample with $N = 4$, in situ nanoindentation in SEM and ex situ SEM analysis was conducted for all samples to compare the morphology of the pile-ups around the nanoindentations. All photographic images were recorded using a nanoindentation facility in an SEM equipped with a

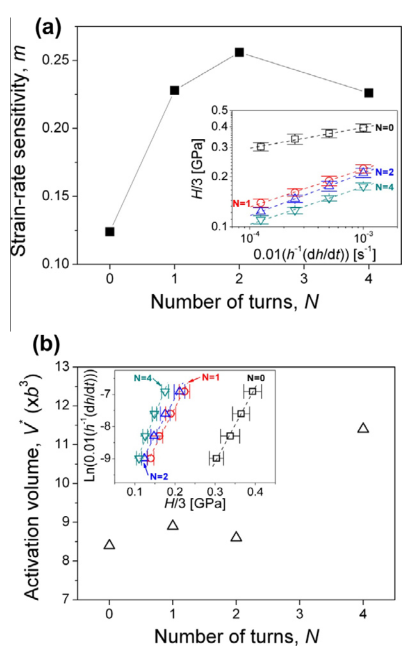

Fig. 3. Variation in (a) strain-rate sensitivity and (b) activation volume with different levels of torsional straining.

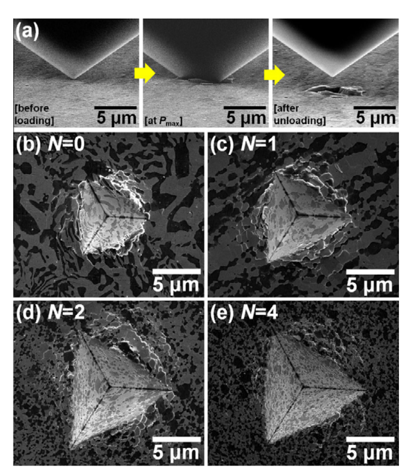

Fig. 4. (a) In situ nanoindentation images of the disk for $N = 0$ under $P_{max} = 10$ mN at $dP/dt = 0.5$ mN s^{-1} and SEM images of the indentations made under $P_{max} = 20$ mN at $\dot{\varepsilon}_i = 0.025$ s^{-1} on the disks for (b) $N = 0$, (c) $N = 1$, (d) $N = 2$ and (e) $N = 4$.

cube-corner indenter which was sharper with a centerline-to-face angle ψ of 35.3° and induced higher stresses and more pronounced pile-up behavior than a standard Berkovich indenter with $\psi = 65.3°$ [27,28].

Figure 4a shows the in situ images for the $N = 0$ sample where the shear-off behavior by GBS is apparent in the pile-up region due to the large grain size. It is generally accepted that the shear-off behavior of ultrafined-grained metals is evidence for GBS and the shear-off unit is close to the grain size [29–31]. Although the shear-off patterns in other samples were not clearly observed during the in situ measurements due to their very fine grains, the ex situ images revealed clear shear-off phenomena for all samples and representative post-mortem indentation images are shown in Figure 4b–e for samples having $N = 0$, 1, 2 and 4 turns, respectively. The increase in indentation size with increasing N confirms the decrease in H with N observed in Figure 2b and, as anticipated, the shear-off behavior in the disk for $N = 4$ reveals less pronounced behavior than in the other disks.

Thus, different levels of GBS are revealed as the dominant deformation mechanism at RT in terms of m and V^* in the Zn–Al alloy during HPT processing through different numbers of revolutions. The reason for the slower GBS in the sample of $N = 4$ can be readily explained. Earlier experiments showed that the contributions of GBS to the plastic deformation was the maximum on the Zn–Zn interfaces and less on the Zn–Al interfaces and the minimum sliding contributions were recorded at the Al–Al interfaces both without [32] and with [33] ECAP. Processing by HPT alters the microstructure from a homogeneous phase distribution to a banded structure after HPT up to 2 turns and this brings an increase in the fraction of the Zn–Zn interfaces [33] and leads to easy GBS with higher m and lower V^*. However, the homogeneous distribution of Al and Zn grains introduced by 4 turns of HPT produces a higher fraction of Zn–Al interfaces and a lower fraction of Zn–Zn interfaces. Therefore, although this sample retains similar ultrafine grains through 2–4 turns, there is a decrease in m and an increase in V^* after 4 turns as shown in Figure 3.

Although a simultaneous decrease or increase in strength (H) and plasticity (m) is not a general feature of coarse-grained metals, such behavior is often found in metals having very small grain sizes such as nanocrystalline or nanotwinned materials where the grain (or twin)-boundary mediated deformation mechanism may be effective in enhancing both H and m [13,14].

This research was supported by the National Research Foundation of Korea (NRF) grant funded by the Korea government (MSIP) (No. 2013R1A1A2A100 58551). The work at USC and the University of Southampton was supported in part by the National Science Foundation of the United States under Grant No. DMR-1160966 and in part by the European Research Council under ERC Grant Agreement No. 267464-SPDMETALS.

[1] P. Kumar, C. Xu, T.G. Langdon, Mater. Sci. Eng. A 429 (2006) 324.
[2] M. Kawasaki, T.G. Langdon, Mater. Trans. 49 (2008) 84.
[3] M. Kawasaki, T.G. Langdon, Mater. Sci. Eng. A 528 (2011) 6140.
[4] R.Z. Valiev, T.G. Langdon, Prog. Mater. Sci. 51 (2006) 881.
[5] A.P. Zhilyaev, T.G. Langdon, Prog. Mater. Sci. 53 (2008) 893.
[6] J. Wongsa-Ngam, M. Kawasaki, T.G. Langdon, J. Mater. Sci. 48 (2013) 4653.
[7] R.Z. Valiev, Yu.V. Ivanisenko, E.F. Rauch, B. Baudelet, Acta Mater. 44 (1996) 4705.
[8] M. Kawasaki, B. Ahn, T.G. Langdon, Acta Mater. 58 (2010) 919.
[9] M. Kawasaki, B. Ahn, T.G. Langdon, Mater. Sci. Eng. A 527 (2010) 7008.
[10] I.-C. Choi, Y.-J. Kim, M.-Y. Seok, B.-G. Yoo, J.-Y. Kim, Y.M. Wang, J.-I. Jang, Int. J. Plast. 41 (2013) 53.
[11] L. Lu, X. Chen, X. Huang, K. Lu, Science 323 (2009) 607.
[12] S. Shim, J.-I. Jang, G.M. Pharr, Acta Mater. 56 (2008) 3824.
[13] I.-C. Choi, B.-G. Yoo, Y.-J. Kim, M.-Y. Seok, Y.M. Wang, J.-I. Jang, Scripta Mater. 65 (2011) 300.
[14] C.L. Wang, Y.H. Lai, J.C. Huang, T.G. Nieh, Scripta Mater. 62 (2010) 175.
[15] R.B. Figueiredo, P.H.R. Pereira, M.T.P. Aguilar, P.R. Cetlin, T.G. Langdon, Acta Mater. 69 (2012) 3190.
[16] M. Furukawa, Z. Horita, M. Nemoto, R.Z. Valiev, T.G. Langdon, J. Mater. Res. 11 (1996) 2128.
[17] W.C. Oliver, G.M. Pharr, J. Mater. Res. 7 (1992) 1564.
[18] M. Kawasaki, J. Mater. Sci. 49 (2014) 18.
[19] I.-C. Choi, Y.-J. Kim, Y.M. Wang, U. Ramamurty, J.-I. Jang, Acta Mater. 61 (2013) 7313.
[20] X. Zhang, H. Wang, R.O. Scattergood, J. Narayan, C.C. Koch, A.V. Sergueeva, A.K. Mukherjee, Acta Mater. 50 (2002) 4823.
[21] H. Miyamoto, K. Ota, T. Mimaki, Scripta Mater. 54 (2006) 1913.
[22] S.H. Xia, J. Wang, J.T. Wang, J.Q. Liu, Mater. Sci. Eng. A 493 (2008) 111.
[23] H. Conrad, Mater. Sci. Eng. A 341 (2003) 216.
[24] H. Conrad, Nanotechnology 18 (2007) 325701.
[25] H.J. Frost, M.F. Ashby, Deformation-mechanism map, Pergamon Press, Oxford, 1982.
[26] T.G. Langdon, F.A. Mohamed, Scripta Metall. 11 (1977) 575.
[27] J.-I. Jang, B.-G. Yoo, Y.-J. Kim, J.-H. Oh, I.-C. Choi, H. Bei, Scripta Mater. 64 (2011) 753.
[28] J.-I. Jang, B.-G. Yoo, J.-Y. Kim, Appl. Phys. Lett. 90 (2007) 211906.
[29] J.M. Wheeler, V. Maier, K. Durst, M. Göken, J. Michler, Mater. Sci. Eng. A 585 (2013) 108.
[30] V. Maier, B. Merle, M. Göken, K. Durst, J. Mater. Res. 28 (2013) 1177.
[31] N.Q. Chinh, P. Szommer, Z. Horita, TG Langdon, Adv. Mater. 18 (2006) 34.
[32] P. Shariat, R.B. Vastava, T.G. Langdon, Acta Metall. 30 (1982) 285.
[33] M. Kawasaki, T.G. Langdon, J. Mater. Sci. 48 (2013) 4730.